Journal of the American Heart Association

ORIGINAL RESEARCH

Metabolic Changes Precede Radiation-Induced Cardiac Remodeling in Beagles: Using Noninvasive ^{18}F-FDG (^{18}F-Fludeoxyglucose) and ^{13}N-Ammonia Positron Emission Tomography/Computed Tomography Scans

Rui Yan, MD*; Xiang Li, MD*; Jianbo Song, MD*; Min Guo, MD; Honghong Cai, MM; Zhifang Wu, MD; Ping Wu, MM; Li Li, MD; Minfu Yang, MD; Yuetao Wang, MD; Sijin Li, MD

BACKGROUND: This study was performed to characterize the metabolic, functional, and structural cardiac changes in a canine model of radiation-induced heart disease by serial in vivo imaging and ex vivo analyses.

METHODS AND RESULTS: Thirty-six dogs were randomly assigned to control or irradiated groups at 3 time points (months 3, 6, and 12 after radiation; each group comprised 6 dogs). The left anterior myocardium of dogs in irradiated groups was irradiated locally with a single dose of 20-Gy X-ray. The irradiated myocardial regions showed increased myocardial uptake of ^{18}F-FDG (^{18}F-fludeoxyglucose) in the irradiated beagles, but the increased uptake area decreased at months 6 and 12 compared with month 3 after radiation. Abnormality of myocardial perfusion and cardiac function were detected at month 6 after radiation. Compared with the control groups, the protein expression of GLUT4 (glucose transporter 4) was upregulated in the irradiated groups, correlating with significantly decreased CPT1 (carnitine acyltransferase 1) expression. Mitochondria degeneration, swelling, and count reduction in the irradiated groups were observed. The difference in CD68 of macrophage markers and the inflammatory cytokines (IL-6 [interleukin 6], TNF-α [tumor necrosis factor α]) between the irradiation and control groups was not significant. Furthermore, the progressive aggravation of apoptosis and fibrosis was displayed.

CONCLUSIONS: Elevated ^{18}F-FDG uptake occurred after irradiation and subsequently led to ventricular perfusion defects and dysfunction. The process was associated with myocardial metabolic substrate remodeling, cardiac muscle cell apoptosis, and myocardial fibrosis rather than inflammation.

Key Words: ^{18}F-FDG PET/CT ■ apoptosis ■ inflammation ■ metabolic substrate remodeling ■ myocardial fibrosis ■ radiation-induced heart disease

Malignant tumors are an important cause of morbidity and mortality worldwide.[1] Radiotherapy was established as monotherapy or adjuvant therapy for different types of malignancies. Improved advances in radiation therapy could increase cancer survival.[2] Nevertheless, radiation-induced heart disease (RIHD) related to micro- and macrovascular damage leads to cardiac manifestations including

Correspondence to: Sijin Li, MD, Department of Nuclear Medicine, First Hospital of Shanxi Medical University, No. 85, Jiefang Road, Taiyuan, Shanxi 030001, China. E-mail: lisjnml23@163.com

Supplementary Material for this article is available at https://www.ahajournals.org/doi/suppl/10.1161/JAHA.120.016875

*Dr Yan, Dr Xiang Li, and Dr Song contributed equally to this work.

For Sources of Funding and Disclosures, see page 10.

JAHA is available at: www.ahajournals.org/journal/jaha

CLINICAL PERSPECTIVE

What Is New?

- Elevated ^{18}F-FDG (^{18}F-fludeoxyglucose) uptakes occurred after irradiation and subsequently led to ventricular perfusion defects and dysfunction.
- The elevated ^{18}F-FDG uptakes were associated with changes in myocardial substrate metabolism rather than inflammation.
- The ventricular perfusion defects and dysfunction were associated with cardiac muscle cell apoptosis and myocardial fibrosis, and adverse metabolic remodeling resulted in the cardiac remodeling of radiation-induced heart disease.

What Are the Clinical Implications?

- ^{18}F-FDG positron emission tomography/computed tomography might be a sensitive method for detecting early radiation-induced myocardial damage.
- Substrate metabolism alternation precedes cardiac remodeling after radiation, which may provide new targets for the treatment of radiation-induced heart disease.

Nonstandard Abbreviations and Acronyms

CPT1	carnitine acyltransferase 1
^{18}F-FDG	^{18}F-fludeoxyglucose
GLUT4	glucose transporter 4
RIHD	radiation-induced heart disease

pericarditis, acute myocardial infarction, or cardiomyopathy, which were widely reported in patients with breast cancer[3] and Hodgkin lymphoma.[4] RIHD was also associated with an increased risk of long-term mortality.[5] Consequently, it is of vital importance to assess potential cardiac complications induced by radiotherapy. Radiation-induced myocardial damage was likely adverse myocardial remodeling in relation to decreased cardiac function without clinical symptoms and ultimately caused heart failure.[6]

In the normal adult heart, fatty acid β-oxidation provides almost 70% of cardiac ATP. However, the failing heart relies more on glucose oxidation than on fatty acid oxidation as the preferred metabolic substrate.[7] The glucose is transported to cardiomyocytes by binding with glucose transporter protein. GLUT4 (glucose transporter 4) is the most abundant glucose transporter in the heart in relation to environmental changes.[7] Proteome study of cardiac tissue response to irradiation found that the most obvious downregulation of proteins was related to fatty acid metabolism.[8,9]

Sensitive and precise quantification for monitoring or predicting early heart adverse effects in the myocardium is demanding.[10] Positron emission tomography (PET) is the gold standard approach for quantitative evaluation of myocardial metabolism and perfusion by glucose analog ^{18}F-FDG (^{18}F-fludeoxyglucose) and ^{13}N-ammonia due to its superior sensitivity and accuracy in diagnosis.[11] There have been limited clinical studies applying cardiac PET to detect pathologic changes in association with RIHD occurrence.

In this study, we serially investigated myocardial ^{18}F-FDG uptake of myocardial glucose metabolism after radiation treatment in correlation with quantitative myocardial perfusion. In addition, biochemical and histologic analyses were performed to determine the tissular mechanism underlying imaging findings.

METHODS

The data that support the findings of this study are available from the corresponding author on reasonable request.

Animals and Experimental Procedures

Thirty-six healthy, 1-year-old, male beagles were provided by Nanjing chaimen Biotechnology Co., Ltd. All animals were placed in stainless steel cages at the Experimental Animal Center of the China Institute for Radiation Protection, in an air-conditioned facilities (18°C–25°C; relative humidity, 40%–60%; ≥12 air changes per hour), fed with standard certified commercial dog chow twice a day, with water available ad libitum. Thirty-six beagles were assigned by random number table method to control groups or irradiated groups at each time point (months 3, 6, and 12 after radiation; each group comprised 6 dogs). The left anterior myocardium of dogs in irradiated groups was irradiated with an X-ray dose of 20 Gy. The control groups underwent sham radiation. Cardiac ^{18}F-FDG PET/computed tomography (CT), ^{13}N-ammonia myocardial perfusion imaging, and biochemical and histologic analysis were performed serially. Experiments were performed in accordance with Chinese national legislation and local guidelines, and animal experimentation was conducted as approved by Shanxi Medical University.

Radiation Procedure

The left anterior myocardium of dogs (irradiated groups) was irradiated with an X-ray dose of 20 Gy. The anterior wall of the left ventricle was outlined as a radiation target in irradiated animals. The targeted volume accounted for a quarter to one-third of left

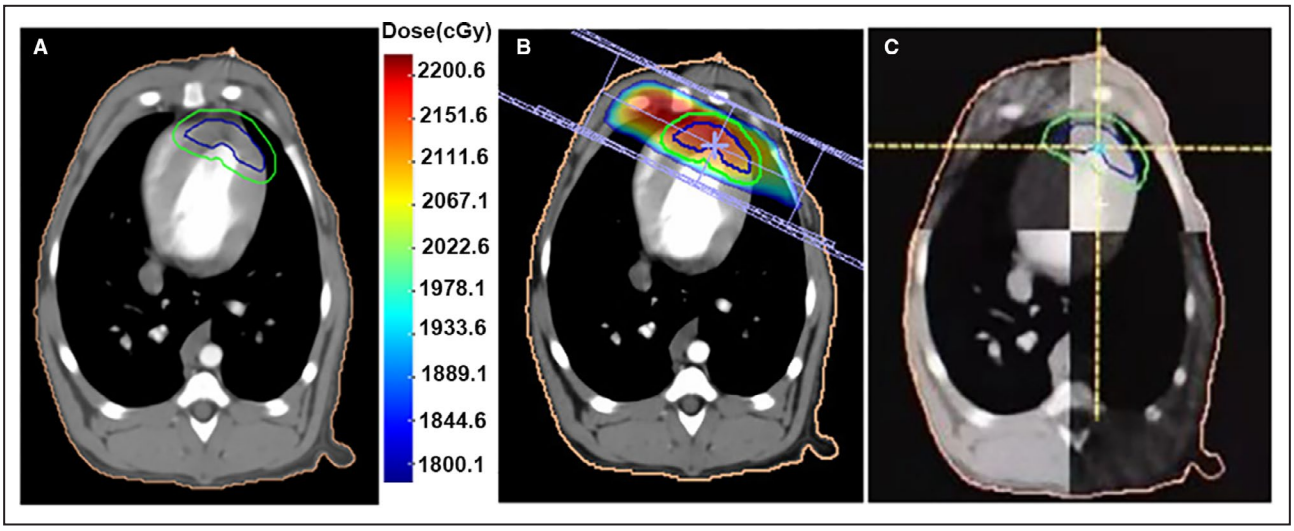

Figure 1. Images of radiation procedure.
A, Irradiation target area. **B**, Radiation-planning images. **C**, Images of position validation by cone-beam computed tomography.

ventricular volume (Figure 1A). Radiation was delivered in the supine position on a linear accelerator unit (Clinac IX; Varian Medical Systems) using a single 20-Gy dose with 6MVX-ray (Figure 1B). Treatment planning was performed by control-enhanced CT (Discovery VCT64 PET/CT; General Electric), and the dose distribution was determined by a Varian Eclipse TPS system. The target area was verified by cone-beam CT scanning with a flat-panel detector (Figure 1C). The dogs in control groups were delivered on a linear accelerator unit without radiation over the same fraction duration.

[18]F-FDG and [13]N-Ammonia PET/CT

After overnight fasting, each dog was subjected to cardiac PET/CT (Discovery VCT; General Electric) after receiving the administration of [13]N-ammonia (148-185 MBq) by intravenous bolus injection. The dogs then received 2 days of high-fat diet and >12 hours of fasting. Subsequently, each dog was subjected to [18]F-FDG administration (3.7–5.5 MBq/kg), and 40 to 60 minutes later, a cardiac PET/CT scan was performed. The prescribed high-fat diet was defined as a diet containing a high-fat content (fat:protein ratio of 9:1) with almost no carbohydrates.

Image Acquisition and Reconstruction

The cardiac PET/CT scan was performed as described previously.[12] The CT scanning conditions were as follows: tube voltage of 120 kV, tube current of 30 mA, and slice thickness of 5 mm. Afterward, PET data (8 phases per cardiac cycle) were acquired using 3D electrocardiography gated mode and the following specifications: 10 minutes of acquisition time, 128 × 128 matrix, iterative reconstruction, 20 data subsets, 2 iterations, and 6-mm full width at half maximum.

Image Analysis

In the semiquantitative analysis of [18]F-FDG imaging, the same sizes of the irradiated and nonirradiated fields were drawn manually as regions of interest. The maximal standardized uptake value of the irradiated field and the nonirradiated field were automatically measured by the Volumetrics software. Then the standardized uptake value ratio of the irradiation field to the nonirradiation field was calculated.

For myocardial perfusion imaging, the radioactivity count of the irradiated and the nonirradiated areas were also automatically measured by the Volumetrics software (Discovery VCT; General Electric). The irradiation:nonirradiation activity ratio was then used to calculate.

[13]N-ammonia PET/CT images were analyzed using Myovation software to calculate the parameters, including left ventricular (LV) end-diastolic volume, LV end-systolic volume, and LV ejection fraction.

Real-Time Quantitative Reverse Transcription Polymerase Chain Reaction

Total RNA from the heart tissue of the dogs was extracted according to the instructions for Trizol reagent (Takara Bio). The cDNA was synthesized using an iScript cDNA synthesis kit (Takara Bio). The cDNA was amplified by a multiple kit (SYBR Premix Ex Taq; Takara Bio) on a StepOnePlus Real-Time PCR System (Thermo Fisher Scientific). The primers are indicated in Table 1. GAPDH served as an internal

Table. Primer Sequences for Real-Time Polymerase Chain Reaction

Gene	Forward Primer (5′ to 3′)	Reverse Primer (5′ to 3′)
CD68	ACCCTGCTGCCCTCCTTCAC	GCCTGGTGAGTGGTGGTGTTG
IL6	CGAGCCCACCAGGAACGAAAG	GAAAGCAGTAGCCATCACCAGGAG
TNF	GGCGTGGAGCTGACAGACAAC	CGAAGCGGCTGATGGTGTGG
GAPDH	AGGAGATGGAACGAGAGGCAGA	CGTGAAGCTGTCGGCATAAGTCC

control.The $2^{-\Delta\Delta Ct}$ method was used to analyze the relative changes in gene expression.

Western Blot Analysis

Total protein was isolated from the LV anterior myocardium of the dogs and the frozen sample using RIPA (Boster Bio). Protein concentration was quantified using the BCA Protein Assay Kit (Boster Bio). Equal amounts of proteins (30 μg) were separated by SDS-PAGE and subsequently transferred electrophoretically to polyvinylidene fluoride (PVDF) membrane. After blocking with 5% skimmed milk at radiotherapy for 4 hours, the membranes were incubated with anti-CPT1 (1:5000; Abcam), anti-SLC2A4 (1:1000; Sigma-Aldrich), anti-CD68 (1:1000; Abcam), and anti-β-actin (1:2000; Abcam) at 4°C overnight, followed by horseradish peroxidase–conjugated secondary antibodies at radiotherapy for 1 hour. Immunoblots were developed with an enhanced chemiluminescence system and quantified by ImageJ software.

Histology

Each dog's heart was subjected to pathologic testing by Masson staining, tunnel staining, and electron microscopy. In detail, tissue samples from the LV anterior myocardium were obtained, fixed in 10% formalin, and embedded in a paraffin block. From each block, 5-mm-thick sections were prepared and stained with Masson trichrome stain and TUNEL (terminal deoxynucleotidal transferase–mediated biotin–deoxyuridine triphosphate nick-end labeling) assay. Tissue samples (1 mm^3) were obtained for electron microscopy, and the specimens were prepared as described previously.[12] Morphologic changes were observed by light microscopy (JEM-2100; JEOL) and transmission electron microscope (JEM-2100; JEOL).

Myocardial fibrosis was analyzed using a Leica-Q 500MC image analysis system (Leica Microsystems) to identify zones of myocardial fibrosis, thereby semiquantitatively determining the collagen volume fraction. Apoptosis detection was performed by TUNEL assay. An apoptotic index expressed as percentage of TUNEL-positive nuclei to total nuclei was calculated.

Statistical Analysis

Continuous variables are expressed as the mean with 95% confidence. Group data were analyzed using 1-way and 2-way ANOVA with Tukey post hoc corrections for multiple comparisons. Statistical analyses were performed using GraphPad Prism 7.0 software. $P<0.05$ was considered statistically significant.

RESULTS

Animals

All dogs underwent the complete experimental process. Radiation was performed precisely, with the error of cone-beam CT analysis consistently <5 mm. No heart failure or death occurred in any dogs.

Radiation Induced Increased Myocardial ^{18}F-FDG Uptake

Neglectable myocardial ^{18}F-FDG uptake was detected in the control groups. However, focal increased ^{18}F-FDG uptake in the anterior of the LV myocardium corresponding to the irradiated field was observed in the irradiated dogs (Figure 2A). Nevertheless, the area of the increased uptake gradually decreased over time (Figure 2B). The standardized uptake value ratio of irradiation related to nonirradiation in the irradiated dogs was significantly higher than in the control groups over time ($P<0.01$) (Figure 2C; Table S1).

Myocardial ^{13}N-Ammonia Uptake Decreased After Irradiation

No abnormal myocardial perfusion was noted in the irradiated myocardial field in the control groups; however, perfusion reduction was observed 6 months after radiation, and perfusion defects were observed 12 months after radiation (Figure 2A). Regional irradiated wall motion abnormalities were observed in 4 dogs at 6 months after radiation and gradually worsened in 6 dogs by 12 months after radiation. In addition, there was a continuously decreased irradiation:nonirradiation activity ratio at 6 and 12 months after radiation compared with the control groups (Figure 2D; Table S1). The irradiated dogs displayed increased myocardial ^{18}F-FDG uptake and myocardial perfusion defects in the anterior wall of the left ventricle.

Radiation Affected Cardiac Dysfunction

Compared with the control groups, irradiated dogs showed that adverse cardiac remodeling in terms of

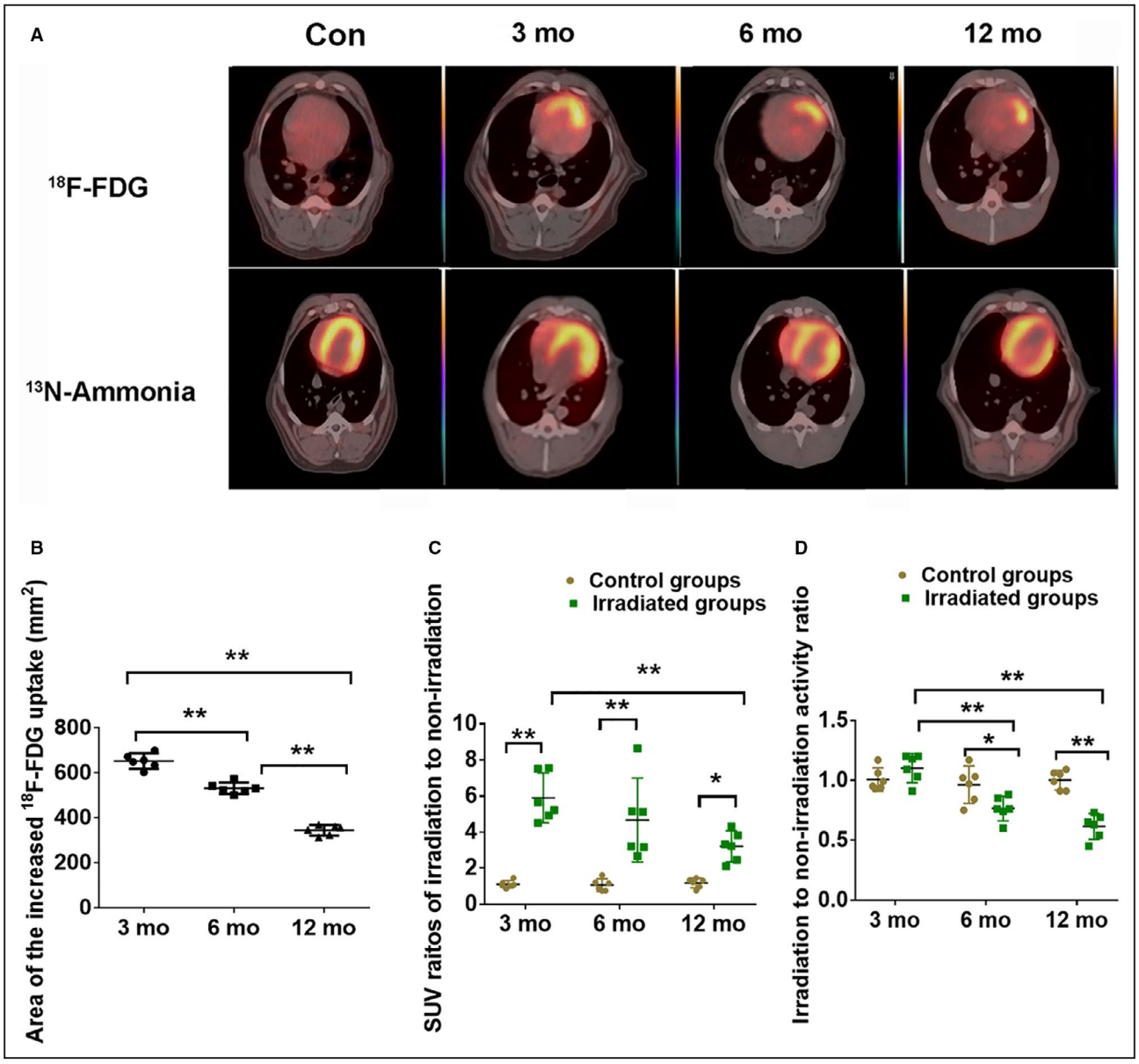

Figure 2. **^{18}F-FDG and ^{13}N-ammonia PET/CT infused images of each group and parameters of PET/CT.**
A, Focal increased ^{18}F-FDG uptake occurred in the irradiated field (upper panel), ^{13}N-ammonia uptake in the irradiated field decreased at month 6 after radiation and disappeared at month 12 after radiation (bottom panel). **B**, Area of increased ^{18}F-FDG uptake. C. Standardized uptake value ratios of irradiation to nonirradiation of ^{18}F-FDG PET/CT. **D**, Irradiation:nonirradiation activity ratio of ^{13}N-ammonia PET/CT. Data are mean with 95% confidence, **P*<0.05, ***P*<0.01. Con indicates control; ^{18}F-FDG, ^{18}F-fludeoxyglucose; PET/CT indicates positron emission tomography/computed tomography; and SUV, standardized uptake value.

enlarged end-diastolic volume and end-systolic volume and a decreased LV ejection fraction were observed at 6 months and gradually deteriorated by 12 months after radiation compared with the control groups (Figure 3; Table S1).

Expression of GLUT4 and CPT1 Proteins in Irradiated Myocardial Region

Compared with the control groups in dogs, the protein expression of GLUT4 increased in irradiated groups. In the meantime, we found that the level of GLUT4 was highest at 3 months after radiation and gradually decreased by 6 and 12 months after radiation. However, protein expression of CPT1 decreased when dogs were exposed to radiation (Figure 4A and 4B; Table S1).

Electron Microscopy After Radiation

The disordered arrangement of myofibrils and some mitochondria swelling were observed in the irradiated group at month 3 compared with the control groups. Myocardial injury was aggravated in the irradiated group at month 6, as shown by apparently disorganized

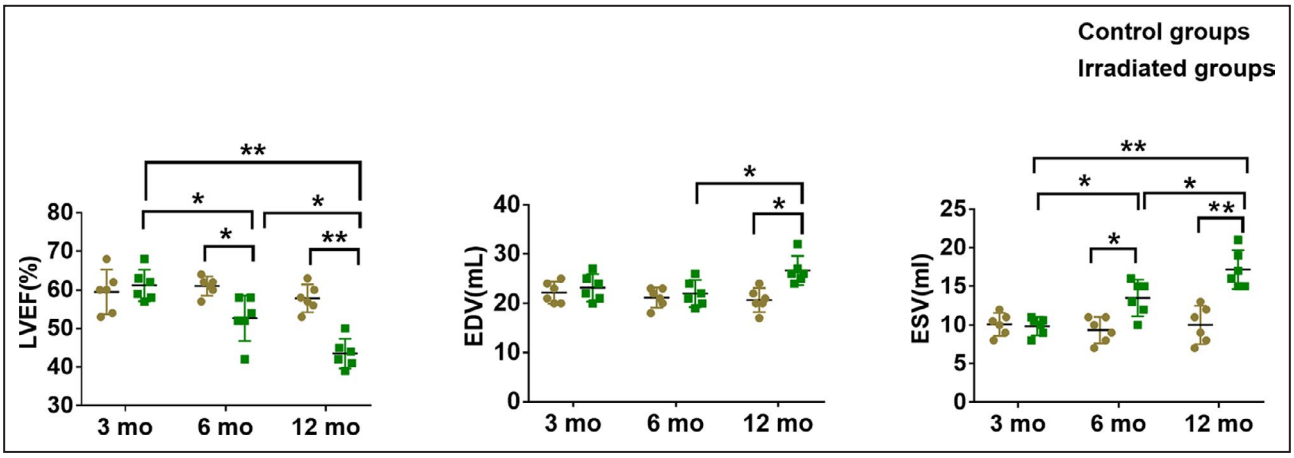

Figure 3. Comparison of functional parameters of the left ventricle in the control and irradiated groups.
The left ventricular ejection fraction (LVEF) was progressively reduced after radiation (left). The ventricular end-diastolic volume (EDV) was increased at month 12 after radiation (middle). The end-systolic volume (ESV) was significantly increased after radiation (right). Data are mean with 95% confidence, **P*<0.05, ***P*<0.01.

myocardial fibers, interstitial fibrosis, and various mitochondrial damage (eg, swelling, degeneration, necrosis, and decreased count). In the irradiated group at month 12, the myocardial damage became more severe, and the interstitial and perivascular fibrosis was even more evident; the mitochondrial swelling and the number decreased were even more obvious (Figure 4C).

Effect of Radiation on CD68 and Inflammation Cytokines

To determine the role of inflammation in the process of increased [18]F-FDG uptake in irradiated myocardium, we also assessed CD68 of macrophage markers and the inflammatory cytokines (IL-6 [interleukin 6], TNF-α [tumor necrosis factor α]) between the irradiation and control groups. As shown in Figure 5 and Table S1, no significant differences in mRNA and protein expression of CD68, IL-6, and TNF-α were observed in irradiated groups compared with the control groups.

Myocardial Fibrosis Aggravated After Irradiation

Our results showed that a clear myocardial fiber texture and almost no collagen staining were seen in the control groups. Pericardial and interstitial fibrosis appeared 3 months after irradiation, and fibrotic tissue gradually increased from 6 to 12 months after irradiation, as determined by Masson staining. Analysis of the images

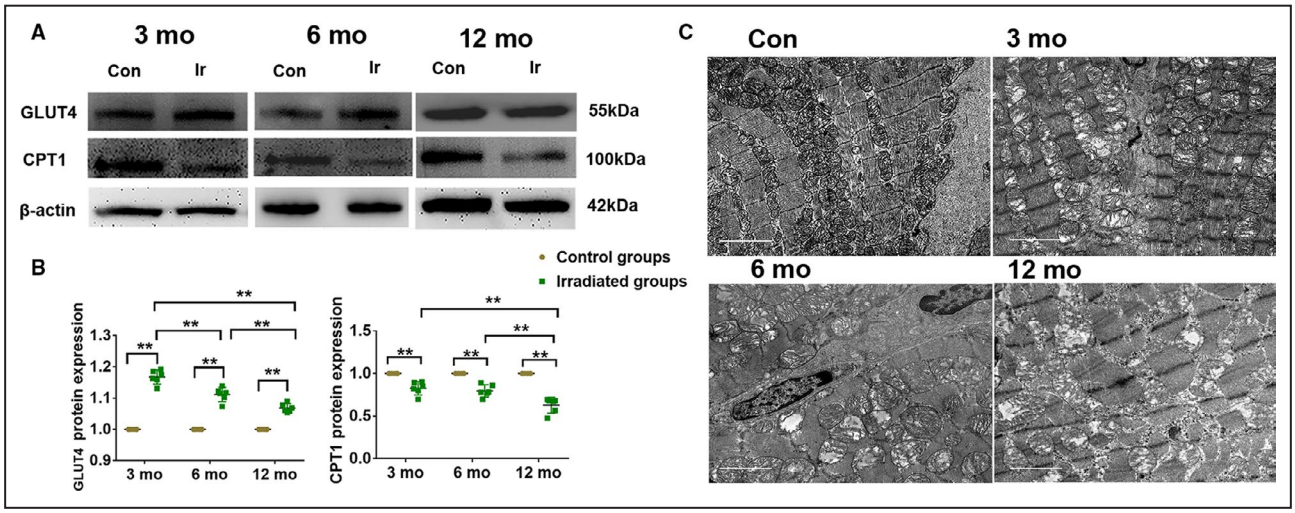

Figure 4. Myocardial metabolic substrate remodeling induced increase of [18]F-FDG uptake.
A, Expression of GLUT4 and CPT1 was determined by western blot. β-actin was a load control. **B**, Data summary of GLUT4 (left) and CPT1 (right) were expressed as broken-line graphs of means with 95% confidence of the independent experiments. **P*<0.05, ***P*<0.01. **C**, Electron microscopy images of the irradiated myocardium of each group, scale bar = 2 μm. Con indicates control; CPT1, carnitine acyltransferase 1; [18]F-FDG, [18]F-fludeoxyglucose; GLUT4, glucose transporter 4; and Ir, irradiated.

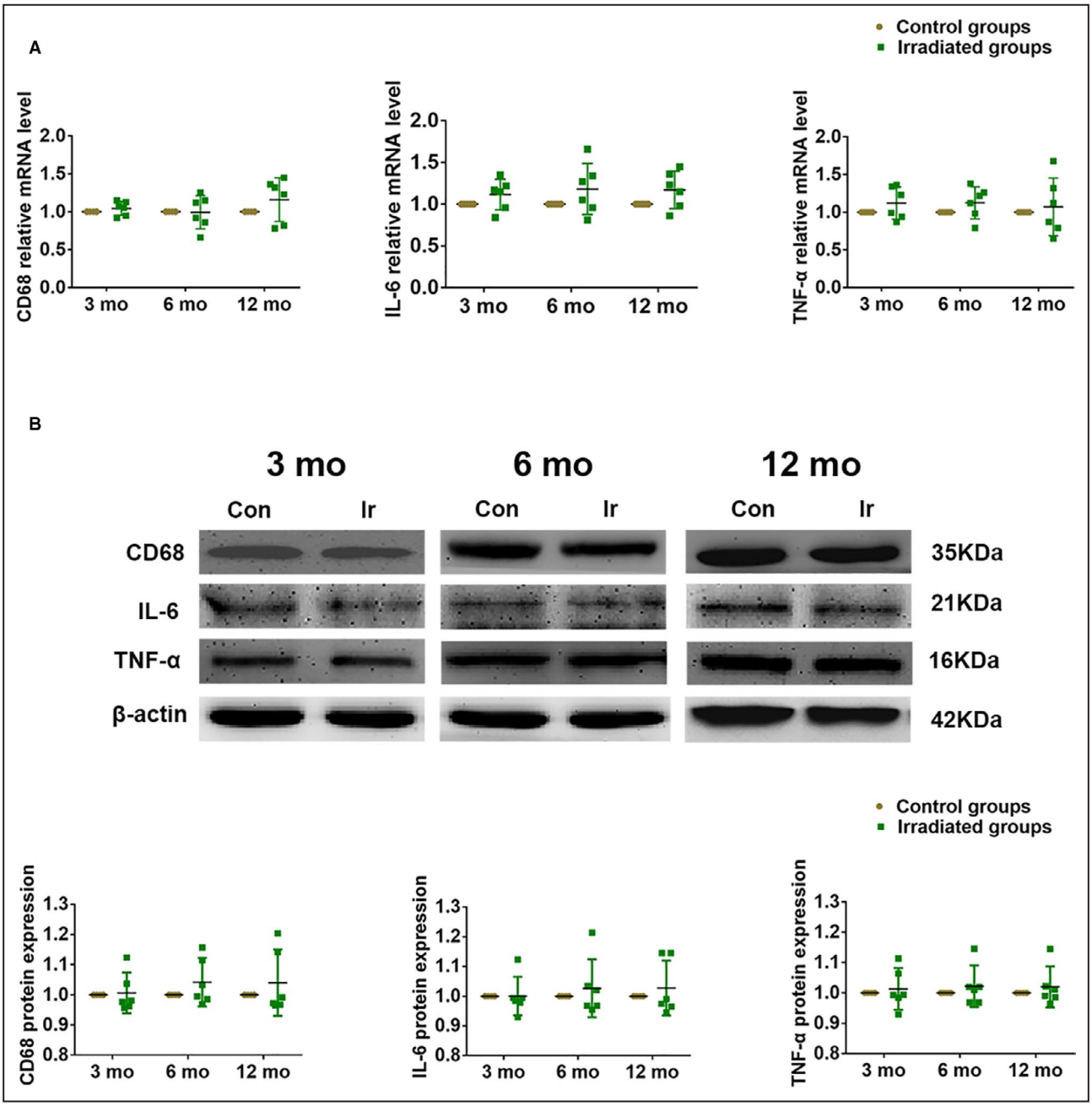

Figure 5. Potential mechanisms of the myocardial inflammation of increased ^{18}F-FDG uptake.
A, The mRNA levels of CD68, IL-6, and TNF-α were measured by quantitative reverse transcription polymerase chain reaction. **B**, The protein expression of CD68, IL-6, and TNF-α were determined by western blot. β-actin was a load control. Quantitative data are presented as mean with 95% confidence. ^{18}F-FDG indicates ^{18}F-fludeoxyglucose; IL-6, interleukin 6; and TNF-α, tumor necrosis factor α.

showed that in comparison to the collagen volume fraction of the control groups, those of the irradiated groups were gradually increased (P<0.01) (Figure 6; Table S1).

Radiation Exacerbated Cardiomyocyte Apoptosis

To further characterize radiation on cardiomyocyte apoptosis, we detected apoptotic cardiomyocytes using TUNEL reaction. TUNEL-positive cells in the control groups were negligible. The number of TUNEL-positive cells was significantly increased in the irradiated group at month 3. A most marked appearance of TUNEL-positive cells was observed in the irradiation group at month 12 compared with other irradiated groups (Figure 7; Table S1).

DISCUSSION

To our knowledge, this study is the first to investigate the metabolic and functional perspectives of

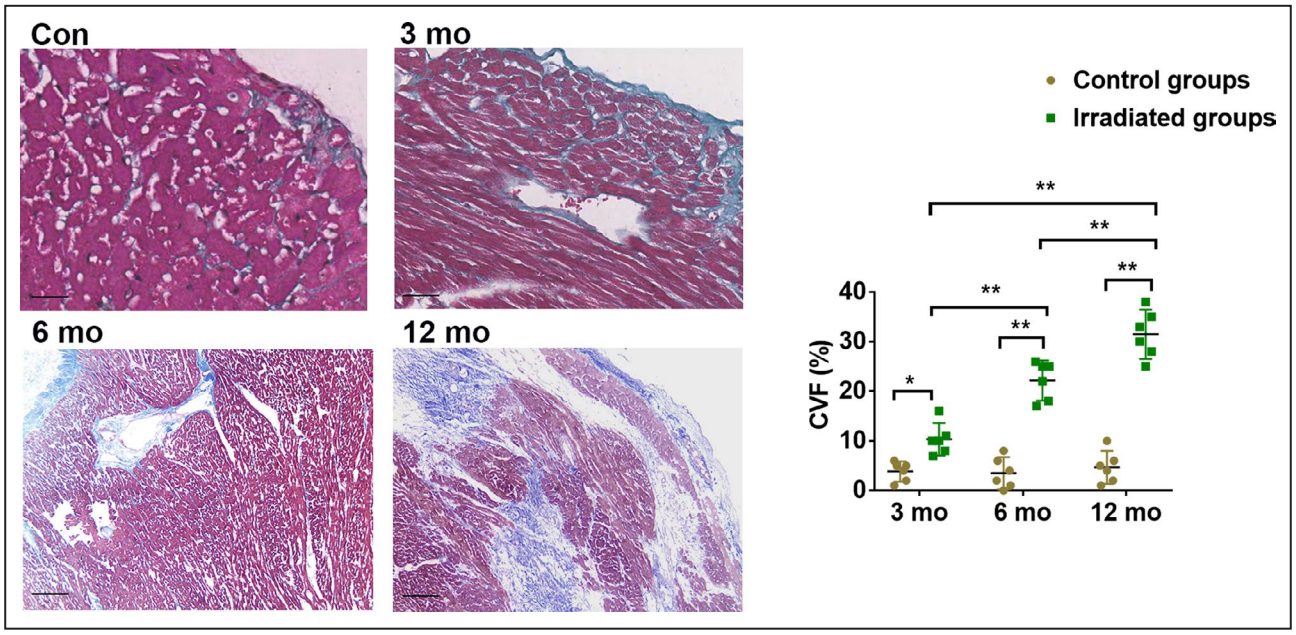

Figure 6. The Masson staining images and CVF of the irradiated myocardium of each group.
Blue staining of collagen fibers were gradually intensified over time. Scale bar = 100 μm, data are mean with 95% confidence, *P<0.05, **P<0.01. Con indicates control; and CVF, collagen volume fraction.

coordinated imaging to determine cardiac damage at cellular and molecular levels. In this study, ^{18}F-FDG uptake serially increased in the irradiated myocardial area after radiation exposure over 12 months in association with the adverse alternation of cardiomyocytes. Meanwhile, adverse cardiac outcomes were exacerbated by gradually impaired myocardial blood flow reserve. Our observations indicated that the regional ^{18}F-FDG uptake in the RIHD might be a sensitive method for detecting early myocardial damage in association with myocardial metabolic substrate remodeling processes.

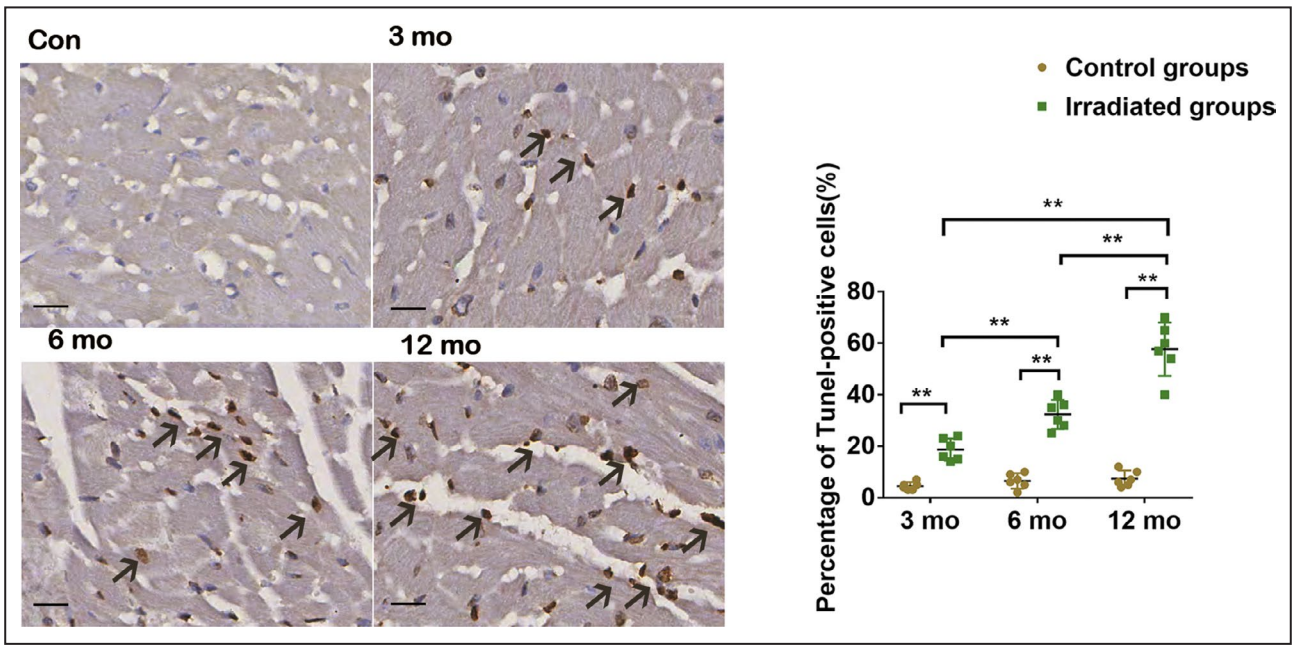

Figure 7. TUNEL assay images and percentage of TUNEL-positive cells of the irradiated myocardium of each group.
The myocardial apoptosis (arrows point to TUNEL-positive nuclei) became aggravated in the irradiated groups at months 3, 6, and 12 compared with the control groups. Scale bar = 50 μm, data are mean with 95% confidence, **P<0.01. Con indicates control; and TUNEL, terminal deoxynucleotidal transferase–mediated biotin–deoxyuridine triphosphate nick-end labeling.

The cardiac radiation effects were well documented in patients with thoracic malignancy. Jingu et al found that 13 of 64 (20.3%) patients with esophageal cancer showed a focal increase in ^{18}F-FDG uptake in the basal myocardium corresponding to the irradiated fields after radiotherapy.[13] Similarly, increasing ^{18}F-FDG foci were detected in irradiated myocardial segments after thoracic radiotherapy.[14,15] Evans et al reported a 47% rate of nonmalignant increased ^{18}F-FDG uptake at irradiated myocardium after stereotactic radiotherapy (20-Gy isodose line >5 cm^3 of the heart).[16] In this study, we simulated clinical high-dose radiation in large animals. Nevertheless, in correlation with the clinical setting, the beagle model of regional heart irradiation was simulated without clinical confounding factors, such as concurrent chemotherapy, and risk factors for cardiovascular disease. Fasting conditions before ^{18}F-FDG PET/CT, in theory, could harm the physiologic metabolism of ^{18}F-FDG in the myocardium. Nevertheless, inconsistent myocardial ^{18}F-FDG uptake was demonstrated under fasting conditions,[17,18] which could compromise the diagnosis of pathologic changes. We introduced a prescan scheme that included 2 days of high-fat diet and subsequent fasting preparation, showing effective suppression of physiologic myocardial ^{18}F-FDG uptake in the control animals (Figure 2B) and removing negative interference with the diagnosis of pathologic changes. Moreover, we serially observed a moderately decreased myocardial flow and contractility at 6 months and then progressive worsening at 12 months after irradiation, suggesting that the increase in ^{18}F-FDG myocardial uptake corresponding to the irradiated field has predictive value regarding radiation-induced myocardial damage.

RIHD began with inflammatory processes that occurred in response to the radiostimulus and accelerated and was sustained longitudinally. This proinflammatory pathogenesis induced by radiation eventually led to endothelial cell proliferation, myocardial collagen deposition, and late regional dysfunctions of the pericardium. The pioneering pathologic study of RIHD in animal models found that there was an inflammatory reaction in the early stage after myocardial radiation but that it was a self-limiting process from the acute to chronic phases, and then it was a process of constant progressive reconstruction.[19–21] In our findings, no difference in proinflammation phenotype macrophage marker CD68 and the inflammatory cytokines was assessed in the irradiated groups compared with the control groups. This demonstrated that focal uptake in irradiated myocardium specifically came from cardiac apoptotic tissue during the chronic phase after cardiac injury.

Regarding the myocardial metabolic substrate, the increased ^{18}F-FDG uptake in irradiated myocardium suggested that the myocardium switched from fatty acid to glucose metabolism as the preferred metabolic substrate. GLUT4 and CPT1 were the major moderators of glucose and fatty acid metabolism, respectively. A radiation-induced overexpression of GLUT4 and suppressed expression of CPT1 in myocardium were observed, resulting in the metabolic substrate alterations of the myocardium. And the reduction in fatty acid oxidation likely occurred because of reduction of overall mitochondrial function and oxidative capacity, as shown by electron microscopy. Under ischemic and hypoxic conditions, GLUT4 is rapidly transported from inside cardiomyocytes to the cell surface.[22] Correspondingly, Umezawa et al found a decrease in fatty acid metabolism in the irradiated myocardium after fatty acid imaging in patients undergoing thoracic radiotherapy for esophageal cancer.[23] Consequently, increased ^{18}F-FDG uptake at the irradiated myocardial area was the result, with myocardial metabolic substrate remodeling. We found that the myocardial area of elevated ^{18}F-FDG uptake was gradually decreased, which had not been reported previously. In concordance, GLUT4 expression steadily decreased over time, resulting in downregulation of glucose metabolism. This pattern of myocardial metabolic alternation was associated with aggravation of local myocardial apoptosis and fibrosis. Because apoptotic myocardium could not absorb ^{18}F-FDG, the area with increased ^{18}F-FDG within the irradiated myocardial area diminished.

Regarding long-term cardiac outcome after radiation, myocardial perfusion defects are related to the time interval following radiation. Visual interpretation could detect perfusion abnormalities in the irradiated areas 6 to 12 months after radiation, which agrees with previous studies.[24,25] In addition, progressive cardiomyocyte apoptosis and myocardial interstitial fibrosis in the irradiated area were detected. Consequently, the ventricular perfusion defects and dysfunction might also be associated with cardiomyocyte apoptosis or myocardial interstitial fibrosis. Mitochondrial dysfunction led to progressive myocardial energy failure, along with decreased myocardial blood flow perfusion. This suggested that adverse metabolic remodeling and myocardial ischemia, which might directly or indirectly promote cardiac fibrosis formation and systolic myocardial dysfunction, could result in cardiac remodeling or heart failure.

Beyond monitoring the cardiac toxicity induced by antimalignant radiotherapy, cardiac ^{18}F-FDG PET might also be effective in the clinic after cardiac stereotactic body radiotherapy for terminating refractory ventricular tachycardias, which could result in adverse cardiac outcomes (eg, heart failure, pericarditis pericardial effusions).[26]

Because symptoms are often nonspecific, patients with radiation-induced cardiac diseases typically present long-term delayed cardiac damage sustained for years after radiation exposure. Our study provides a valuable coordinated imaging method to monitor disease severity or therapeutic response.

Limitations

This study has the following limitations. First, no myocardial fatty acid imaging was performed at the same time. However, we observed that decreased the level of CPT1 in the irradiated groups and was sustained up to 12 months after radiation; the data initially reflected myocardial metabolic remodeling by radiation. Furthermore, tumors may occasionally undergo cardiac metastasis that results in an increase in ^{18}F-FDG uptake in the metastatic myocardial tissue[27]; therefore, it is clinically necessary to determine the cause of increased ^{18}F-FDG uptake.

CONCLUSIONS

Elevated ^{18}F-FDG uptake occurred after irradiation and subsequently led to ventricular perfusion defects and dysfunction. Furthermore, the process was associated with myocardial metabolic changes rather than inflammation, which lead to the remodeling of cardiac muscle cell apoptosis and myocardial fibrosis. This study may provide new targets for the diagnosis and treatment of RIHD.

ARTICLE INFORMATION

Received April 5, 2020; accepted July 10, 2020.

Affiliations

From the Department of Nuclear Medicine of First Hospital (R.Y., X.L., H.C., Z.W., P.W., L.L., S.L.), and Department of Cardiology of First Hospital (M.G.), Shanxi Medical University, Taiyuan, China; Department of Radiotherapy, Shanxi Bethune Hospital (Shanxi Academy of Medical Sciences), Taiyuan, China (J.S.); Division of Nuclear Medicine, Department of Biomedical Imaging and Image-Guided Therapy, Medical University of Vienna, Vienna, Austria (X.L.); Department of Nuclear Medicine, Beijing Chao-Yang Hospital, Capital Medical University, Beijing, China (M.Y.); Department of Nuclear Medicine, The Third Affiliated Hospital of Soochow University, The First People's Hospital of Changzhou, Changzhou, China (Y.W.); and Province-Ministry Co-construction Cooperative Innovation Center of Precise Diagnosis and Treatment of Molecular Image, Taiyuan, China (S.L.).

Acknowledgments

We give special thanks for the technical support from the Institute of Radiation Protection in China.

Sources of Funding

This study was supported by grants from the Natural Science Foundation of China (81671724), the Natural Science Foundation for Young Scientists of Shanxi Province, China (201701D221251), the Natural Science Foundation of Shanxi Province, China (201801D121337), and Startup Foundation for Doctors of Shanxi Medical University (03201553).

Disclosures

None.

Supplementary Material

Table S1

REFERENCES

1. Siegel R, Miller K, Jemal A. Cancer statistics, 2017. *CA Cancer J Clin*. 2017;67:7–30.
2. Rosenblatt E, Izewska J, Anacak Y, Pynda Y, Scalliet P, Boniol M, Autier P. Radiotherapy capacity in European countries: an analysis of the directory of radiotherapy centres (dirac) database. *Lancet Oncol*. 2013;14:e79–e86.
3. Recht A. Radiation-induced heart disease after breast cancer treatment: How big a problem, and how much can-and should-we try to reduce it? *J Clin Oncol*. 2017;35:1146–1148.
4. Aleman B, van den Belt-Dusebout A, De Bruin M, van't Veer MB, Baaijens M, Boer J, Hart A, Klokman WJ, Kuenen MA, Ouwens G, et al. Late cardiotoxicity after treatment for hodgkin lymphoma. *Blood*. 2007;109:1878–1886.
5. Dent S, Liu P, Brezden-Masley C, Lenihan D. Cancer and cardiovascular disease: the complex labyrinth. *J Oncol*. 2015;2015:516450.
6. Liu H, Xiong M, Xia Y, Cui N, Lu R, Deng L, Lin Y, Rong T. Studies on pentoxifylline and tocopherol combination for radiation-induced heart disease in rats. *Int J Radiat Oncol Biol Phys*. 2009;73:1552–1559.
7. Stanley WC, Recchia FA, Lopaschuk GD. Myocardial substrate metabolism in the normal and failing heart. *Physiol Rev*. 2005;85:1093–1129.
8. Azimzadeh O, Sievert W, Sarioglu H, Yentrapalli R, Barjaktarovic Z, Sriharshan A, Ueffing M, Janik D, Aichler M, Atkinson MJ, et al. Ppar alpha: a novel radiation target in locally exposed mus musculus heart revealed by quantitative proteomics. *J Proteome Res*. 2013;12:2700–2714.
9. Subramanian V, Seemann I, Merl-Pham J, Hauck SM, Stewart FA, Atkinson MJ, Tapio S, Azimzadeh O. Role of TGF beta and PPAR alpha signaling pathways in radiation response of locally exposed heart: Integrated global transcriptomics and proteomics analysis. *J Proteome Res*. 2017;16:307–318.
10. Curigliano G, Cardinale D, Dent S, Criscitiello C, Aseyev O, Lenihan D, Cipolla C. Cardiotoxicity of anticancer treatments: epidemiology, detection, and management. *CA Cancer J Clin*. 2016;66:309–325.
11. Awadalla M, Hassan MZO, Alvi RM, Neilan TG. Advanced imaging modalities to detect cardiotoxicity. *Curr Probl Cancer*. 2018;42:386–396.
12. Yan R, Song J, Wu Z, Guo M, Liu J, Li J, Hao X, Li S. Detection of myocardial metabolic abnormalities by 18F-FDG PET/CT and corresponding pathological changes in beagles with local heart irradiation. *Korean J Radiol*. 2015;16:919–928.
13. Jingu K, Kaneta T, Nemoto K, Ichinose A, Oikawa M, Takai Y, Ogawa Y, Nakata E, Sakayauchi T, Takai K, et al. The utility of 18F-fluorodeoxyglucose positron emission tomography for early diagnosis of radiation-induced myocardial damage. *Int J Radiat Oncol Biol Phys*. 2006;66:845–851.
14. Unal K, Unlu M, Akdemir O, Akmansu M. 18F-FDG PET/CT findings of radiotherapy-related myocardial changes in patients with thoracic malignancies. *Nucl Med Commun*. 2013;34:855–859.
15. Zöphel K, Hölzel C, Dawel M, Hölscher T, Evers C, Kotzerke J. PET/CT demonstrates increased myocardial FDG uptake following irradiation therapy. *Eur J Nucl Med Mol Imaging*. 2007;34:1322–1323.
16. Evans J, Gomez D, Chang J, Gladish G, Erasmus J, Rebueno N, Banchs J, Komaki R, Welsh J. Cardiac 18F-fluorodeoxyglucose uptake on positron emission tomography after thoracic stereotactic body radiation therapy. *Radiother Oncol*. 2013;109:82–88.
17. Inglese E, Leva L, Matheoud R, Sacchetti G, Secco C, Gandolfo P, Brambilla M, Sambuceti G. Spatial and temporal heterogeneity of regional myocardial uptake in patients without heart disease under fasting conditions on repeated whole-body 18F-FDG PET/CT. *J Nucl Med*. 2007;48:1662–1669.
18. Giorgetti A, Marras G, Genovesi D, Filidei E, Bottoni A, Mangione M, Emdin M, Marzullo P. Effect of prolonged fasting and low molecular weight heparin or warfarin therapies on 2-deoxy-2-[18f]-fluoro-d-glucose pet cardiac uptake. *J Nucl Cardiol*. 2018;25:1364–1371.
19. Fajardo LF, Stewart JR. Experimental radiation-induced heart disease. I. Light microscopic studies. *Am J Pathol*. 1970;59:299–316.
20. Boerma M. Experimental radiation-induced heart disease: past, present, and future. *Radiat Res*. 2012;178:1–6.

21. Steiner I. Pathology of radiation induced heart disease. *Rep Pract Oncol Radiother*. 2020;25:178–181.
22. Davey K, Garlick P, Warley A, Southworth R. Immunogold labeling study of the distribution of glut-1 and glut-4 in cardiac tissue following stimulation by insulin or ischemia. *Am J Physiol Heart Circ Physiol*. 2007;292:H2009–H2019.
23. Umezawa R, Takase K, Jingu K, Takanami K, Ota H, Kaneta T, Takeda K, Matsushita H, Ariga H, Takahashi S, et al. Evaluation of radiation-induced myocardial damage using iodine-123 beta-methyl-iodophenyl pentadecanoic acid scintigraphy. *J Radiat Res*. 2013;54:880–889.
24. Song J, Yan R, Wu Z, Li J, Yan M, Hao X, Liu J, Li S. (13)n-ammonia pet/ct detection of myocardial perfusion abnormalities in beagle dogs after local heart irradiation. *J Nucl Med*. 2017;58:605–610.
25. Sioka C, Exarchopoulos T, Tasiou I, Tzima E, Fotou N, Capizzello A, Ragos V, Tsekeris P, Fotopoulos A. Myocardial perfusion imaging with (99 m)tc-tetrofosmin spect in breast cancer patients that received post-operative radiotherapy: a case-control study. *Radiat Oncol*. 2011;6:151.
26. Robinson CG, Samson PP, Moore KMS, Hugo GD, Knutson N, Mutic S, Goddu SM, Lang A, Cooper DH, Faddis M, et al. Phase i/ii trial of electrophysiology-guided noninvasive cardiac radioablation for ventricular tachycardia. *Circulation*. 2019;139:313–321.
27. Malik D, Basher R, Vadi S, Mittal B, Bhattacharya A. Cardiac metastasis from lung cancer mimicking as perfusion defect on n-13 ammonia and fdg myocardial viability pet/ct scan. *J Nucl Cardiol*. 2017;24:1442–1444.

SUPPLEMENTAL MATERIAL

Table S1. Baseline Characteristics.

	3 month (95% CI)			6 month (95% CI)			12 month (95% CI)			*P* value (Ir)		
	Con (n=6)	Ir (n=6)	*P* value	Con (n=6)	Ir (n=6)	*P* value	Con (n=6)	Ir (n=6)	*P* value	3mo Vs 6mo	3mo vs 12mo	6mo vs 12mo
Male	6	6	NA	6	6	NA	6	6	NA	NA	NA	NA
Area of the increased ^{18}F-FDG uptake (mm^2)	653.32 (618.41-688.23)			532.48 (506.71-558.26)			345.91 (322.54-369.28)			<0.0001	<0.0001	<0.0001
SUV ratios of irradiation to non-irradiation	1.12 (0.91-1.32)	5.90 (4.52-7.29)	<0.0001	1.07 (0.71-1.42)	4.67 (2.34-6.99)	<0.0001	1.18 (0.92-1.45)	3.22 (2.35-4.08)	0.0399	0.4175	0.0032	0.2492
Irradiation to non-irradiation activity ratio	1.01 (0.91-1.10)	1.10 (0.98-1.22)	0.6577	0.96 (0.81-1.12)	0.77 (0.66-0.87)	0.0378	1.00 (0.92-1.08)	0.62 (0.51-0.72)	<0.0001	0.0001	<0.0001	0.1912
LVEF(%)	59.50 (53.72-65.28)	61.17 (56.90-65.44)	0.9846	61.00 (58.52-63.48)	52.67 (46.49-58.85)	0.0263	57.83 (54.23-61.43)	43.50 (39.48-47.52)	<0.0001	0.0224	<0.0001	0.0116

EDV(mL)	22.17 (19.92-24.41)	23.17 (20.40-25.94)	>0.9999	21.17 (19.13-23.20)	22.00 (19.26-24.74)	>0.9999	20.67 (18.21-23.12)	26.67 (23.72-29.61)	0.0027	0.9997	0.2425	0.0345
ESV(ml)	10.08 (8.58-11.58)	9.85 (8.66-11.04)	>0.9999	9.33 (7.62-11.05)	13.50 (11.13-15.87)	0.0119	10.00 (7.52-12.48)	17.17 (14.65-19.69)	<0.0001	0.0401	<0.0001	0.0386
GLUT4 protein expression	1	1.17 (1.14-1.19)	<0.0001	1	1.11 (1.09-1.13)	<0.0001	1	1.07 (1.05-1.08)	<0.0001	<0.0001	<0.0001	<0.0001
CPT1 protein expression	1	0.83 (0.75-0.91)	<0.0001	1	0.80 (0.72-0.87)	<0.0001	1	0.63 (0.53-0.72)	<0.0001	0.9221	<0.0001	0.0001
CD68 relative mRNA level	1	1.05 (0.95-1.14)	0.9954	1	0.99 (0.76-1.22)	>0.9999	1	1.16 (0.86-1.46)	0.4714	0.9912	0.7800	0.4267
IL-6 relative mRNA level	1	1.12 (0.92-1.31)	0.8972	1	1.18 (0.86-1.50)	0.5713	1	1.17 (0.94-1.41)	0.6278	0.9871	0.9938	>0.9999
TNF-α relative mRNA level	1	1.12 (0.90-1.35)	0.9271	1	1.13 (0.90-1.35)	0.9190	1	1.07 (0.67-1.47)	0.9925	>0.9999	0.9983	0.9977
CD68 protein expression	1	1.01 (0.94-1.07)	>0.9999	1	1.04 (0.96-1.12)	0.8203	1	1.04 (0.93-1.15)	0.8446	0.8966	0.9145	>0.9999

IL-6 protein expression	1	1.00 (0.93-1.07)	>0.9999	1	1.03 (0.92-1.13)	0.9737	1	1.03 (0.93-1.12)	0.9691	0.9751	0.9707	>0.9999
TNF-α protein expression	1	1.01 (0.94-1.08)	0.9964	1	1.02 (0.95-1.09)	0.9602	1	1.02 (0.95-1.09)	0.9740	0.9993	0.9998	>0.9999
CVF (%)	3.83 (1.80-5.87)	10.33 (7.04-13.63)	0.0293	3.50 (0.27-6.73)	22.17 (18.11-26.23)	<0.0001	4.67 (1.30-8.03)	31.50 (26.50-36.50)	<0.0001	<0.0001	<0.0001	0.0007
Percentage of Tunel-positive cells(%)	4.50 (2.91-6.09)	18.67 (14.18-23.15)	0.0012	6.50 (3.48-9.52)	32.33 (26.45-38.22)	<0.0001	7.33 (4.10-10.56)	57.67 (46.79-68.55)	<0.0001	0.0018	<0.0001	<0.0001